J8.6 MOUNTAIN WAVE STRUCTURES OCCURRING WITHIN A MAJOR OROGRAPHIC PRECIPITATION EVENT: PART II. EVALUATION OF MESOSCALE MODEL SIMULATIONS

Matthew F. Garvert, B. Smull, and C.F. Mass
[1]Department of Atmospheric Sciences, University of Washington, Seattle, WA, 98195, USA

1. INTRODUCTION

Over the past decade, a significant increase in computational power has advanced the ability to use mesoscale models for real-time and research simulations at high resolution. Experience indicates that mesoscale models, when run at sufficiently high resolution, are often capable of simulating accurately the complex kinematic and dynamical structures associated with mountainous terrain (Colle and Mass 1996; Steenburgh and Mass 1996; Doyle et al. 2000). Additionally, increased model resolution (down to 4 km), has been shown to improve the distribution of surface precipitation over major barriers (Colle and Mass 1999; Colle et al. 1999a,b). Yet there are still major problems with high-resolution quantitative precipitation forecasts (QPF), with some studies suggesting significant overprediction present on the windward slopes and often underprediction in the lee. Colle and Mass (1999) identified the need to make improvements to the model's moist physics, particularly the microphysical parameterizations.

To investigate the errors in model QPF, several studies have focused on mesoscale models' bulk microphysical parameterizations (BMPs). Such studies have utilized two-dimensional models to investigate sensitivities of BMPs, or simply focused on the differences in surface precipitation and mixing ratios using different BMPs (Colle 2004; Thompson et al. 2004). Most of these studies, however, have lacked a comprehensive set of observations to isolate errors in the models parameterizations of microphysical processes from problems with basic state kinematic and dynamical fields.

The second phase of the Improvement of Microphysical PaRameterization through Observational Verification Experiment (IMPROVE-2) provided a unique opportunity to examine microphysical processes over topography and assess the validity of present day numerical model BMPs (Stoelinga et al. 2003). The IMPROVE-2 field experiment, which took place in November and December 2001 over the Oregon Cascades, collected a comprehensive set of observations that provided a detailed depiction of the thermodynamic and kinematic structure of many precipitation events. The collection of kinematic and thermodynamic data simultaneously with microphysical measurements provides a unique opportunity to isolate potential problems in the model BMP from other possible model errors in the dynamic representation of the storm systems.

Corresponding author's address: Matthew Garvert, University of Washington Seattle, WA, 98195,USA;
E-Mail: mgarvert@atmos.washington.edu

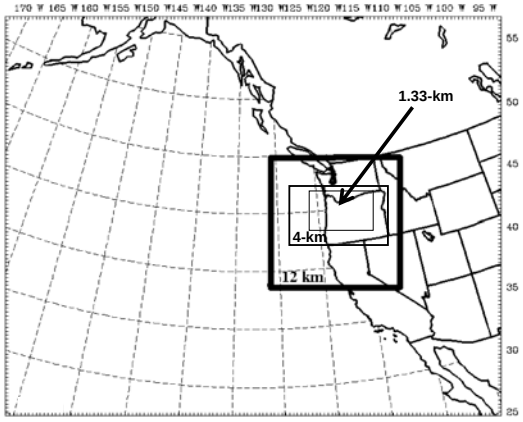

Figure 1. Map of the Pacific Northwest with the 36-km, 12-km, 4-km, and 1.33-km MM5 domains delineated by boxes.

This paper is the second in a two part series. Part-1 (Smull et al. 2005) presented a unique dual-Doppler data-set and assessed the amplitude and strength of mountain waves on several distinct scales on both the lee and windward slopes from a fully three-dimensional perspective for a three hour period during the 13-14 December 2001 IMPROVE-2 case. In this paper, output from the National Center for Atmospheric Research (NCAR) /Pennsylvania State University (PSU) Mesoscale Model (MM5) will be evaluated alongside the dual-Doppler observations and then employed to examine the evolution of these standing waves. Model sensitivity studies will assist in deconstructing the complex interaction between the upstream flow field and the mountain wave over the crest. Finally, details of the precipitation structures and modeled surface precipitation fields as they relate to the mountain waves will be examined.

2. MESOSCALE MODEL DESCRIPTION

The PSU-NCAR Mesoscale Model (MM5) version 3.6 was employed in non-hydrostatic mode to simulate the 13-14 December 2001 system. A 36-km outer domain with a 12-km nest was run for 36 hours covering a large area of the eastern Pacific and Pacific Northwest (Fig 1). The model was initialized at 0000 UTC 13 December 2001 by interpolating a modified National Center for Environmental Prediction (NCEP) Aviation Model (AVN) initialization for 0000 UTC 13 December 2001 to the outermost MM5 grid. The 0000 UTC 13 December AVN grid was improved by

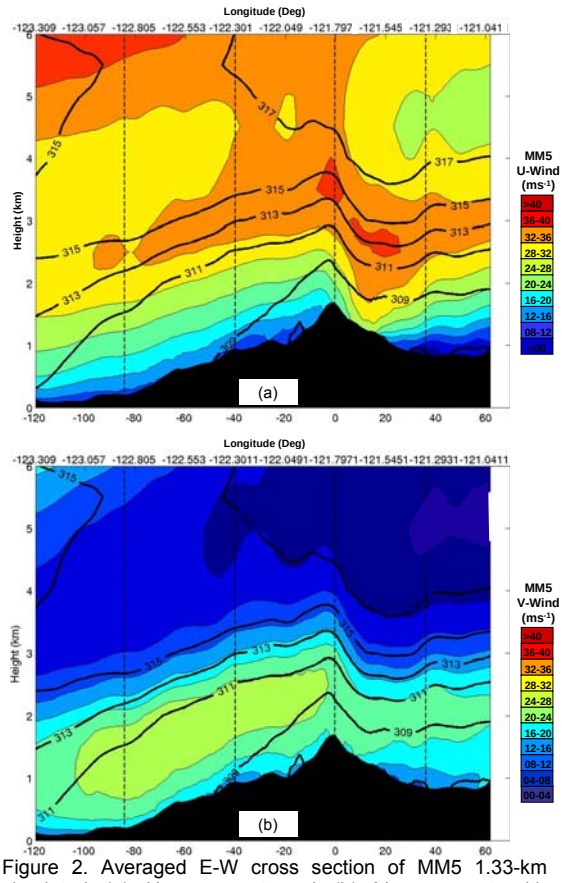

Figure 2. Averaged E-W cross section of MM5 1.33-km simulated (a) U-component and (b) V-component with contours of simulated equivalent potential temperature (θ_e). Model fields were averaged in time from 2300 UTC-0100 UTC 13-14 December 2001 (forecast hours 10-13) using model output at 15 minute intervals.

Incorporating surface and upper-air observations using a Cressman-type analysis scheme (Benjamin and Seamen 1985). Additional analyses were generated every six hours using similarly modified AVN initialization and forecast grids and then linearly interpolating in time to provide lateral boundary conditions every six hours for the 36-km domain. To ensure the most accurate simulation, four-dimension data assimilation (FDDA) was employed on the outer domains during the first twenty-four hours of the forecast.

Thirty-two unevenly spaced full-sigma levels were used in the vertical, with maximum resolution in the boundary layer. The simulation used the updated (version 3.6) explicit moisture scheme of Reisner 2 (Thompson et al. 2004), Grell cumulus parameterization (Grell 1993) and the MRF planetary boundary layer scheme (Hong and Pan 1996). In addition to the 36 and 12 km domains, a separate 4-km simulation with a 1.33-km nest centered over the central Oregon Cascades was run for 24-hours initialized at 1200 UTC 13 December 2001 (Fig 1). The 4-km grid was initialized by linearly interpolating forecasts from the 12-km MM5 simulation. The 4 and 1.33 km domains did not employ nudging or cumulus parameterizations.

3. ANALYSIS OF MODEL KINEMATIC FIELDS

3.1 Windward Slopes

Mean E-W cross sections (analogous to Fig. 3a,b in Part-I) were created using the U- and V- fields from the MM5-1.33-km simulation (Fig 2a,b). The model cross-sections were also averaged for the time period of the P3 flight, from 2300 UTC through 0100 UTC 13-14 December 2001 (forecast hours 11-13) at 15 minute interval model output. The MM5 successfully simulated the broad characteristics of the orographically modified flow, including the low-level U-component shear and the core of stronger U above the shear layer. The model also simulated the strong V-component of winds at low-levels and the decrease of V with height above 2-3 km.

Yet there were also problems with the simulation's representation of the flow kinematics over the windward slopes. The strength of U-shear was underpredicted, with low-level U-values being too strong while the U was 5-8 m s^{-1} too weak above 2-km. Additionally, the height of the modeled U-wind shear layer over the windward slopes was about 0.5 km lower than observed. Low-level V-component values were also 4-6 m s^{-1} stronger than those observed, with the elevated core of maximum V values extending farther east toward the crest. Despite these differences however, the MM5 simulation provided generally realistic depiction of the flow characteristics upwind of the Cascade crest.

In addition to the MM5 U and V-values, simulated equivalent potential temperature (θ_e) contours are also plotted in Fig. 2. Values of θ_e as opposed to potential temperature, θ, are depicted because θ_e is conserved during both dry- and saturated-adiabatic processes. Since the environment during the 13-14 December case was close to saturation up to 4-km (Garvert et al. 2005a), the θ_e contours can be treated as tracers of the steady-state flow, with the exception of areas where other diabatic processes (such as the melting) occur.

The model-depicted low θ_e values are banked up against the crest of the Cascades coincident with the layer of decreased cross-barrier winds. Lower values of θ_e (and θ not shown) near the surface are consistent with reflectivity observations from the P3 radar which showed the bright-band or melting layer descending in height with approach to the Cascade crest (cf. Fig 3c in Part-I). An enhanced vertical θ_e gradient was found atop the zone of lower U-winds and within the zone of enhanced U aloft. Strong V-winds were present below the θ_e gradient and rapidly decreased with height above (Fig. 2b), indicating that the cooler air stream was predisposed to flow more nearly parallel to the Cascade range.

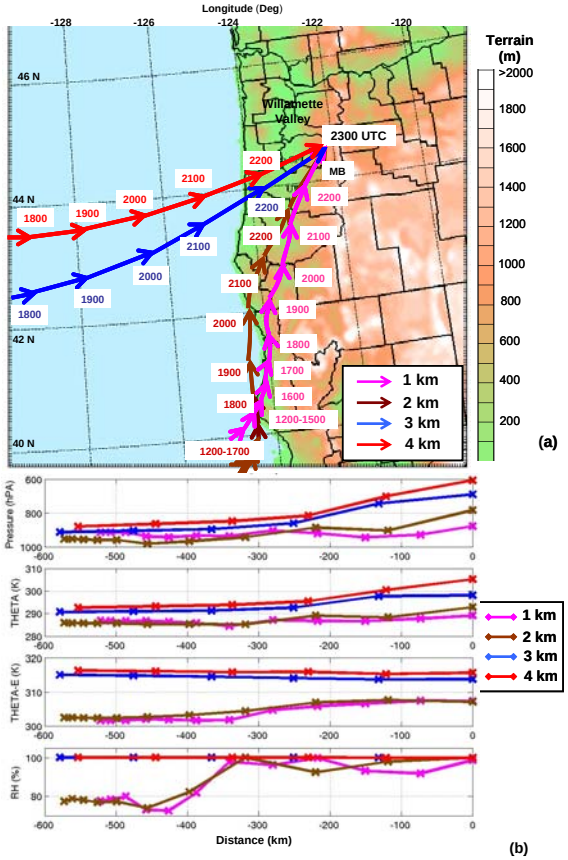

Figure 3: (a) Map of backward trajectories terminating over the windward slopes of the Cascades (at point -122.8 ^{0}N and 44.5 ^{0}W) at 2300 UTC 13 December 2001 at four different heights (key lower right). Lagrangian traces of pressure (hPa), potential temperature (K), equivalent potential temperature (K), and relative humidity (in percent) following the parcel tracks shown in (a), plotted against distance (km) from endpoint.

Trajectories were calculated to determine the origin of the low θ_e air banked up against the windward slopes of the Cascades using a more expansive 4-km MM5 domain simulation. Figure 3a shows the locations of four trajectories ending at hour 2300 UTC (forecast hour 12). All terminate at the same horizontal location (44.3^{0}N and -122.3^{0}W) but at different heights ranging from 1 to 4 km. These trajectories were calculated using 600s time steps from MM5 4-km hourly output. Lagrangian values of pressure, θ, θ_e, and relative humidity values for the four trajectories are displayed in Fig.3b.

The parcel trajectory ending at a height of 1-km nearly paralleled the Cascades at a relatively constant pressure-level of 910-hPa from 1200-2300 UTC 13 December. This parcel was sub-saturated from 1200-1800 UTC 13 December 2001, although relative humidities increased from 75 to 90 percent along the northward track. From 1800-2300 UTC, the parcel's relative humidity remained close to 100 percent as it neared the zone of enhanced orographic precipitation over the IMPROVE study area. The values of θ_e and θ for this parcel showed a 5-6^{0}K increase during its northward trajectory. The parcel ending at 2-km also followed a similar course, originating to the south-southwest of the endpoint off the coast of California. The 2-km parcel remained at a pressure level of around 950hPa between 1200 and 2000 UTC and then rose to 784-hPa as it encountered the higher terrain of the foothills. The θ and θ_e of the 2-km trajectory experienced a 5^{0}K increase during the 4-hours, indicating warming.

The two parcels that reached heights of 3 and 4-km both originated within a distinctly different air mass and region than the lower trajectories. Both upper level trajectories began over the Pacific to the west-southwest of the study-area in a nearly saturated airmass exhibiting higher θ_e values near 317 ^{0}K. The 3- and 4-km parcels experienced significantly more ascent than those paralleling the terrain, rising over 225-hPa in less than five hours. These elevated parcels' θ_e remained relatively steady while θ dramatically warmed due to release of latent heat via condensation.

3.1 Crest and Lee Slopes

The MM5 simulated the stronger U-momentum air over the windward slopes plunging downward with height to the lee of the Cascade crest (Fig. 2b). The modeled 32 m s^{-1} contour line lowered by approximately 1.2-km over a horizontal distance of 10-km from the crest to the lee, which is comparable in amplitude to the observed displacement. However the simulated core of strong U-momentum reached much closer to the ground and spanned a larger horizontal downstream distance than observed. Such errors in the model depiction of the mountain wave can have significant implications on the precipitation distribution to the lee of the Cascade-crest; Garvert et al. 2005b identified this lee region as an area of significant overprediction of surface precipitation rates. The unrealistically strong shunting of precipitation earthward by this displaced wave motion may have contributed to such overprediction in the lee.

To assess the impact of the upstream boundary and shear layer on the mountain wave over the crest, a variety of sensitivity tests were conducted using different planetary boundary layer parameterization (PBL) schemes available in MM5. The control simulation was run with the MRF-PBL parameterization which utilizes the Troen-Mahrt representation of the countergradient term (Hong and Pan 1996). A second run was performed identical to the control but using the Eta-PBL parameterizations on the inner 4- and 1.33-km domains. The Eta-PBL which is used in the operational Eta-model (Janjic 1990,1994), is a 1.5 order closure scheme in which turbulent kinetic energy (TKE) is predicted with a prognostic energy equation, as adapted from the Mellor-Yamada scheme.

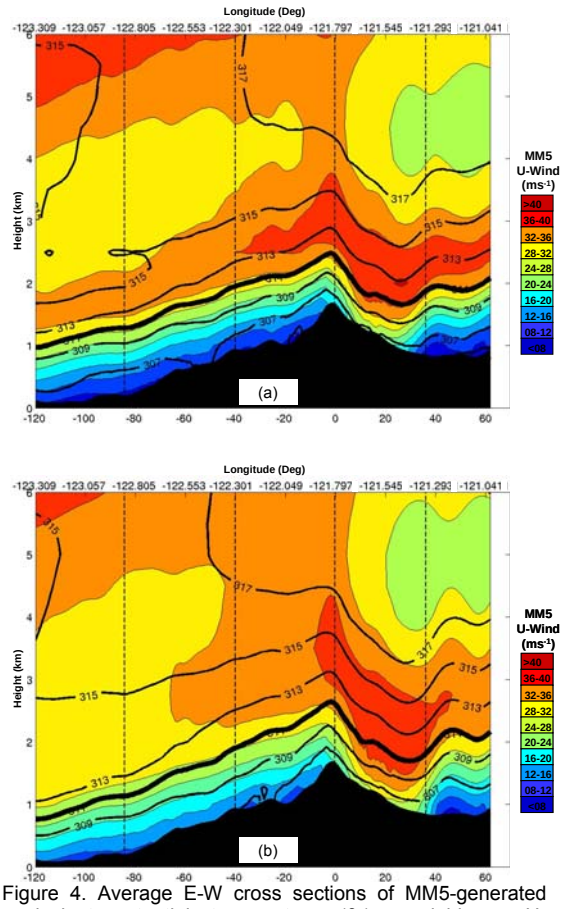

Figure 4. Average E-W cross sections of MM5-generated equivalent potential temperature (θ_e) overlaid on U-component flow for two different 1.33-km MM5 simulations using the (a) ETA-PBL and (b) Yonsei PBL. Model fields were averaged in time from 2300 UTC-0100 UTC 13-14 December 2001 (forecast hours 10-13) using model output at 15 minute interval.

The depth of the low θ_e air and shear layer over the windward slopes in the Eta-PBL simulation was significantly reduced compared to the control run (Fig. 4a and Fig 2a). The resulting windward shear-layer was also stronger than that in the control simulation, better matching observations. Yet, in contrast to the dual-Doppler observations, the Eta-PBL simulation brought stronger U-momentum values closer to the surface and over a wider area to the lee of the Cascade-crest. Additionally, the wave structures as depicted by vertical velocity (not shown) in the Eta-simulation were significantly different than those in the control, with higher amplitude vertical motions evident in the lee.

A third simulation was performed using a modified version of the MRF-PBL (referred to an Yonsei-PBL) as outlined in Noh et al. 2003. The Yonsei-PBL produced similar results to the Eta-PBL simulation, reducing the depth of the upstream shear layer and increasing the amplitude of the lee wave response (Fig. 4b). The Yonsei-PBL, however, did not increase the strength of the shear-layer as significantly as the Eta-simulation.

4. MODEL PRECIPITATION STRUCTURES

4.1 Larger scale (>20 km) Precipitation Features

To determine the origin of the prominent reflectivity features in Part-I, predicted cloud liquid water (CLW) and snow (qs) fields were averaged using 15-minute interval data from 2300-0100 UTC 13-14 December 2001 and overlain on the observed Doppler reflectivity fields (Fig. 5a,b). By comparing these modeled based mixing ratios with the airborne Doppler data, the origins of these reflectivity structures can be better ascertained. Remarkably, averaged model fields indicated corresponding increases in the amount of CLW at 100 and 70 km upstream of the crest, over virtually the same regions where the reflectivity perturbations occurred (Fig. 5a). The fact that the perturbations in CLW were clearly evident even after averaging over a 2-hour period, indicates the stationary and fixed nature of the reflectivity perturbations.

Experiments were performed (not shown) to determine the effects of the coastal mountains and terrain resolution had on the reflectivity and precipitation patterns over the upstream areas. It was demonstrated that without the coastal mountains (Noco) the modeled CLW maximum centered at 100-km upstream of the crest over the Willamette valley was absent when compared to the control simulation. This difference between the Noco and control runs indicated the presence of a lee-wave produced by the coastal mountains which enhanced precipitation over the Willamette Valley. A smoothed-terrain simulation clearly illustrated the sensitivity of the windward mountain waves and microphysical responses to the steepness of the underlying terrain over the windward slopes.

Collocated with the higher reflectivity values over the Cascade-crest, simulated maximum snow mixing ratios (>0.9 g kg^{-1}) extended from 40-km upstream of the crest to the immediate lee (Fig 5b). The enhanced snow mixing ratios and observed reflectivities originated in an area of dendritic growth and strong vertical ascent associated with the mountain wave over the mean crest. The high snow mixing ratios were sequentially advected beyond (i.e. east) the barrier in the strong cross-barrier flow before being dumped to the immediate lee of the Cascades by the strong downward motion within a profound mountain-induced gravity wave. The strong gradient in snow mixing ratio to the lee of the Cascades was in very close agreement an observed reduction of radar reflectivity values.

This precipitation signal resulted in reduced modeled precipitation amounts near the crest and an area of markedly enhanced precipitation amounts in the immediate lee (not shown). Although this

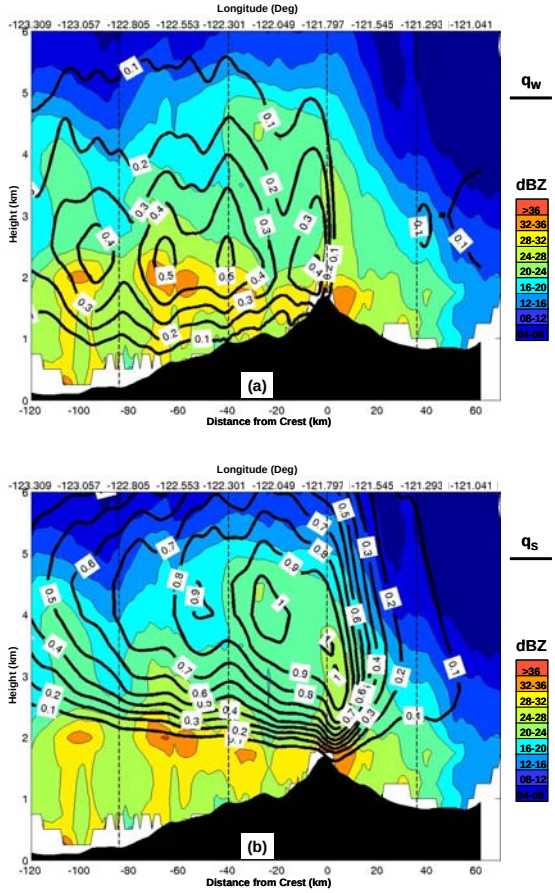

Figure 5. Average E-W cross section of MM5-1.33 km modeled (a) cloud liquid water (q_w) and (b) snow (q_s) in g kg^{-1} overlaid on airborne dual-Doppler derived radar reflectivity (color shading, key right). The modeled CLW and q_s shown were averaged in time from 2300 UTC-0100 UTC 13-14 December 2001 (forecast hours 10-13) using model output at 15 minute intervals.

precipitation distribution could not be extensively verified, an examination of precipitation amounts from 1400-0800 UTC 13-14 December 2001 [cf. Fig. 16 of Garvert et al. 2005b] did indicate some tendency for a reduced precipitation totals near the crest versus over the windward slopes and immediate lee.

4.2 Smaller scale (<20 km) Precipitation Features

On smaller scales > 20 km, significant perturbations in vertical velocity were present over the foothills as the strong low-level V-component flow interacted with the complex terrain of the windward slopes as seen in Fig. 4 of Part I. The MM5 V-component flow along leg-2 (Fig. 6a) was in general agreement with observations showing significant shear both V below 3-km. As mentioned previously, the model simulation exhibited notable errors in this zone, including low-level V-winds 5-8 m s^{-1} too strong below 3-km. Despite these errors, the model's vertical velocity field compared well with the observations (c f. Fig 4a of Part I.), simulating the dramatic oscillations associated with the strong V-values interacting with the complex terrain along leg-2. The model vertical velocity oscillations were stronger than the smoothed Doppler-derived w, consistent with analysis of the in situ data in Garvert et al. 2005b. These simulated w-oscillations also showed greater vertical penetration, which was probably closer to reality given the artificial boundary conditions w=0 at echo top imposed in the derivation of the Doppler-derived vertical velocity field.

Model depictions of the precipitation and CLW fields over leg-2 of the P3 flight-track (Fig. 6b) showed the complex microphysical interactions produced by the strong vertical velocity perturbations. Pockets of high CLW were present over the individual ridges coincident with the areas of strong upward vertical velocity. Where the upper level-snow field intersected with the high CLW pockets, riming of the snow particles and graupel formation above the freezing level was simulated by the model. The higher fallspeeds of the rimed snow particles and graupel resulted in the enhancement of the bright-band over the crest as the particles fell through the melting layer. The increase in precipitation amounts was illustrated by the higher mixing ratios of rain (>0.4 g kg^{-1}) over the crest and to the immediate lee of several of the ridges. The precipitation distribution at the surface was therefore very sensitive to the amount of riming, the fallspeed of the particles, and the phase and amplitude of the small-scale waves.

5. CONCLUSION

This study applies a combination of high-resolution mesoscale model simulations and uniquely comprehensive airborne Doppler radar observations to identify essential kinematic structures influencing the production and mesoscale distribution of precipitation (and associated microphysical quantities) characterizing a period of heavy pre-frontal orographic rainfall over the Oregon Cascades on 13-14 December 2001 during IMPROVE-2. The thermodynamic underpinnings of the terrain-modified flow are explored via parcel trajectory analysis. This approach identifies a tendency for relatively warm, most westerly flow originating over the eastern Pacific to ascend over an effective barrier represented by sub-crest layer of drier, potentially cooler air being channeled northward along and immediately upstream of the Cascade crest, in a manner analogous to that identified by Rotunno and Ferretti (2001) for an Alpine flooding event.

Two distinct scales of mesoscale wave-like air motions are clearly identified: (1) a profound vertically-propagating mountain wave anchored to the meridionally extensive Cascade crest in association with strong baroclinically-induced midlevel cross-barrier zonal flow, and (2) smaller-scale (<20 km wavelength) undulations over the windward foothills

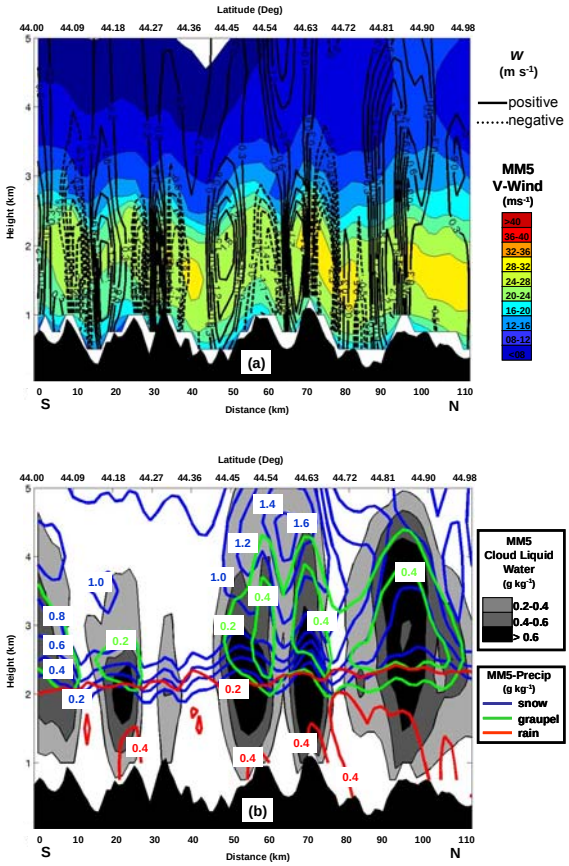

Figure 6. S-N cross-sections along leg 2 of (a) MM5-simulated vertical velocity (m s^{-1}) overlaid on MM5 V-component winds and (b) contours of modeled snow, graupel, and rain mixing ratios in g kg^{-1}. Shaded regions in (b) denote areas where model predicted CLW mixing ratios exceeded 0.2 g kg^{-1} .

triggered by interaction of the ageostrophic along-barrier flow with multiple ridge--valley corrugations oriented perpendicular to the Cascade crest. These undulations are related to persistent modulation of cloud-liquid water (CLW) and snow mixing-ratio within MM5, which in turn compare favorably to radar-documented zones of enhanced reflectivity.

Extension of radar-detectable precipitation echo from well upstream of the Cascades into the lee allows depiction of terrain-induced wave motions in unprecedented detail. Documented errors in the vertical placement (though not necessarily amplitude) of the more profound crest-anchored mountain wave likely contributed to overprediction of lee-slope precipitation rates in MM5. The errors in the mountain wave may have been due to the model's tendency to underestimate the depth and strength of vertical shear exhibited by cross-barrier flow ascending the windward slopes. Sensitivity tests indicate the problem was extremely sensitive to changes in the planetary boundary layer (PBL) parameterization scheme being applied.

Further analysis (presented in Garvert et al. 2006), of model QPF between 2200-0100 UTC showed the small-scale waves increased the modeled precipitation amounts over the windward slopes by 4-14% over a smoothed terrain model simulation. Yet during this 3-hour period, the smoothed terrain resolution did not significantly alter the total amount of precipitation over the domain, but instead redistributed the precipitation in different areas. When a longer 18 hour period which included pre-frontal, frontal, and postfrontal precipitation regimes, was considered the total precipitation amount over the entire domain showed a net increase of 8% for the original terrain compared to the smoothed simulation. This increase appeared to be directly tied to an increase in precipitation over the windward slopes caused by the smaller-scale wave perturbations. Additional work will be required to understand fully the impact that these smaller-scale perturbations have on the precipitation amounts over the windward slopes. Specifically, idealized model simulations that can better isolate and quantify the microphysical processes and resulting surface precipitation patterns will likely be required.

Additional information on the IMPROVE-project and related papers can be found at ***http://improve.atmos.washington.edu/***

6. ACKNOWLEDGEMENTS

This research was funded by the National Science Foundation.

7. REFERENCES

Benjamin, S,G and N.L. Seamen, 1985 :A simple scheme for objective analysis in curved flow. *Mon. Wea. Rev*., **84**, 1184-1198

Colle B. 2004: Sensitivity of orographic precipitation to changing ambient conditions and terrain geometries: An idealized modeling perspective. *J. Atmos. Sci.*, **61**, 588-606

_____, M. F. Garvert, J. Wolfe, C. F. Mass, and C. Woods 2005: 13-14 December 2001 IMPROVE-2 Event. Part-3. Microphysical Budgets and Sensitivity Studies, *J. Atmos. Sc*i. (IMPROVE Special Issue), In Press.

_____, C. F. Mass,1999 The 5-9 February 1996 flooding event over the Pacific Northwest: Sensitivity studies and evaluation of the MM5 precipitation forecasts., **128**, 593-617.

_____ K,Westrick, C.F. Mass 1999a: Evaluation of MM5 and ETA-10 precipitation forecasts over the Pacific Northwest during the cold season. *Weather and Forecasting*: **14**, 137-154.

_____ , K., Westrick, C.F. Mass., 1999b: MM5 Precipitation Verification over the Pacific Northwest during the 1997–99 Cool Seasons**.** *Weather and Forecasting*: **15**, No. 6, pp. 730–744.

_____, C. F. Mass, 1996, An Observational and Numerical Study of a Cold Front Interacting with the Olympic Mountains during COAST IOP5**.** *Monthly Weather Review* **12,** 1310–1334.

Doyle, J.D. and others., 2000: An intercomparison of model-predicted wave breaking for the 11 January 1972 Boulder windstorm. *Mon. Wea. Rev*.,**128**,901-914

Garvert, M. F., B. A. Colle, and C. F. Mass, 2005a: The 13-14 December 2001 IMPROVE-2 Event. Part 1: Synoptic and mesoscale evolution and comparison with a mesoscale model simulation. *J. Atmos. Sci.* (IMPROVE Special Issue),In Press.

_____, C.P. Woods,B. A. Colle, C. F. Mass, P.V. Hobbs, M.P. Stoelinga and J. Wolfe 2005b: The 13-14 December 2001 IMPROVE-2 Event. Part 2:.: Comparisons of MM5 Model Simulations of Clouds and Precipitation with Observations *J. Atmos. Sci.* (IMPROVE Special Issue), IN Press.

_____, B. Smull, and C. F. Mass, 2006: Mountain Wave structures occurring within a major orographic precipitation event. *J. Atmos. Sci.* Submitted

Grell, George. 1993: Prognostic Evaluation of Assumptions Used by Cumulus Parameterizations. *Monthly Weather Review*: Vol. 121, No. 3, pp. 764–787

Hong, Song-You, Pan, Hua-Lu. 1996: Nonlocal Boundary Layer Vertical Diffusion in a Medium-Range Forecast Model. *Monthly Weather Review*: Vol. 124, No. 10, pp. 2322–2339.

Janjic Z. I. 1990: The step-mountain coordinate: Physical Package. *Mon. Wea. Rev*.,**118,** 1429-1443

Janjic Z. I. 1994: The step-mountain coordinate model: Further developments if convection, viscous sublayer, and turbulence closure schemes. *Mon. Wea. Rev*.,**122,** 927-945

Medina S., B. Smull, R.A. Houze, M. Steiner 2005: Cross Barrier Flow During Orographic Precipitation Events: Results from MAP and IMPROVE. *J. Atmos. Sci.* (IMPROVE Special Issue),In Press.

Noh Y. and others, 2003: Improvement of the K-profile model for the planetary boundary layer based on large eddy simulation data. *Boundary Lay. Meteor*., **107**, 401-427.

Rotunno. R. and R. Ferretti, 2001: Mechanisms of intense alpine Rainfall. *J. Atmos. Sci..*, **58**, 1732-1750.

Smull, B, M. Garvert, C F. Mass 2005, Mountain wave structures occurring within a major orographic precipitation event: Part I. Analysis of Airborne Doppler Radar Data:. *32rd Conference on Radar Meteorology,* AMS, Albuquerque, NM

Steenburgh, J and C. Mass, 1996: Interaction of an intense extratropical cyclone with coastal orography. *Mon Wea. Rev*, **124,**1329-1352.

Stoelinga, M., P. V. Hobbs, C. F.Mass, J. D.Locatelli, B. A. Colle, and co-authors, 2003: Improvement of microphysical parameterizations through observational verification experiments (IMPROVE). *Bull. Amer. Meteor. Soc*., **84,** 1807-1826.

Thompson, G., R. M., Rasmussen, and K. Manning, 2004: Explicit forecasts of winter precipitation using an improved bulk microphysics scheme. Part I: Description and Sensitivity Analysis. *Mon. Wea. Rev*. **132**, 519-542.

Woods, C. P., M. T. Stoelinga, J. D. Locatelli, and P. V. Hobbs, 2005: Microphysical Processes and Synergistic Interaction between frontal and orographic forcing of precipitation during the December 13, 2001 IMPROVE-2 event over the Oregon Cascades. *J. Atmos. Sci.* (IMPROVE Special Issue), In Press.